A&A 376, 112–123 (2001)
DOI: 10.1051/0004-6361:20010818

Astronomy & Astrophysics

SiO maser survey of AGB stars in the North Galactic Cap⋆

Y. Ita[1], S. Deguchi[2], T. Fujii[4], O. Kameya[3,4], M. Miyoshi[3,4], Y. Nakada[1,5], J. Nakashima[6], and M. Parthasarathy[7,8]

[1] Institute of Astronomy, School of Science, The University of Tokyo, 2-21-1 Osawa, Mitaka, Tokyo 181-0015, Japan
[2] Nobeyama Radio Observatory, National Astronomical Observatory, Minamimaki, Minamisaku, Nagano 384-1305, Japan
[3] Mizusawa Astrogeodynamics Observatory, National Astronomical Observatory, Mizusawa, Iwate 023-0861, Japan
[4] VERA project office, National Astronomical Observatory, Mitaka, Tokyo 181-8588, Japan
[5] Kiso Observatory, School of Science, The University of Tokyo, Mitake, Kiso, Nagano 397-0101, Japan
[6] Department of Astronomical Science, The Graduate University for Advanced Studies, Nobeyama Radio Observatory, National Astronomical Observatory, Minamimaki, Minamisaku, Nagano 384-1305, Japan
[7] National Astronomical Observatory, 2-21-1 Osawa, Mitaka, Tokyo 181-8588, Japan
[8] Indian Institute of Astrophysics, Bangalore 560034, India

Received 4 December 2000 / Accepted 1 June 2001

Abstract. A SiO maser survey in the $J = 1-0$, $v = 1$ and 2 transitions has been made for IRAS sources in the North Galactic Cap ($b > 30°$) with the Nobeyama 45 m radio telescope. The sources were selected on the basis of their IRAS 12/25-μm and 25/60-μm flux ratios as likely oxygen-rich AGB candidates. SiO masers were detected from 24 out of the 97 selected sources, where 17 were new detections. The distances and heights above the Galactic plane are calculated. The Galactic distribution of detected and undetected stars indicates that metallicity is likely to govern the detection rate. The Galactocentric angular velocities of the subsampled stars are derived and their variation with the Galactic height is discussed.

Key words. late-type star – radio lines – galactic kinematics and structure

1. Introduction

SiO masers have been detected from late-type stars of considerably different types of variability and wide range of mass-loss rates. The widespread occurrence of SiO masers among different classes of Asymptotic Giant Branch (AGB) stars, including those with very low mass-loss rates (e.g., $\sim 10^{-8}$ $M_\odot$ yr^{-1} for R Leo, Lane et al. 1987), indicates that unlike OH and H_2O, SiO masers are likely to arise from the innermost regions of their circumstellar envelopes. Recent interferometic observations show that SiO masers are indeed located very close to the central star (e.g., Cohen 1989; Miyoshi et al. 1994). Also, the pumping mechanism for SiO masers proposed by Deguchi & Iguchi (1976) predicts that the maser beam is directed tangentially to the radial outflows. This implies that the central velocity of the SiO maser line equals the line of sight (l.o.s.) velocity of the star within a few km s^{-1} accuracy (Jewell et al. 1991; Jiang et al. 1995). Therefore, it is a powerful tool for investigating stellar radial velocities.

Up to now, SiO maser surveys have been made, for example, toward the Galactic Bulge (Nakada et al. 1993; Izumiura et al. 1994, 1995a, 1995b), toward the outer disk of the Galaxy (Jiang et al. 1996). In spite of the many SiO maser observations, little attention has been paid to stars in the North Galactic Cap. This region is very interesting because one has an easier access to the thick disk population and can investigate the nature of its constituent stars.

In this paper, we present the result of the SiO maser survey of the AGB stars in the North Galactic Cap. Based on this result, we discuss the spatial distribution of the high galactic latitude maser sources. Also, based on the

Send offprint requests to: Y. Ita,
e-mail: yita@mtk.ioa.s.u-tokyo.ac.jp

⋆ Based on observations at the Nobeyama Radio Observatory (NRO). NRO is a branch of the National Astronomical Observatory, an inter-university research institute, operated by the Ministry of Education, Science and Culture, Japan.

l.o.s. velocities, we discuss the vertical kinematics of the Galaxy.

2. Source selection

The IRAS Point Source Catalog (IRAS PSC) (IRAS Science Team 1988) is at present still the most comprehensive catalog of IR sources, although more comprehensive all sky NIR survey data, e.g., the Two Micron All Sky Survey, is recently getting available in part. Therefore, stars which satisfy all of the four following criteria

1. $b > 30°$;
2. $f_{12} > 3$ (Jy);
3. $-0.301 < C_{12}\ (\equiv \log\,[f_{25}/f_{12}]) < 0.6$;
4. $C_{23}\ (\equiv \log\,[f_{60}/f_{25}]) < -0.48$,

were selected from version 2 of the IRAS PSC, where b is the galactic latitude and f_λ denotes the flux density in Jansky in wavelength λ as detected by IRAS. As a result, the sample studied here consists of 97 IRAS sources.

In the direction away from the plane, there are many observational advantages; (1) one has reliable IRAS 60 and 100 μm measurements, (2) interstellar extinction can be reasonably neglected, and (3) there is no point source confusion.

The selected stars are listed in Table 1, together with their IRAS flux density ratios. Also (l, b) calculated from the IRAS position, IRAS LRS spectral class (LRS), the pulsation periods, and the SiO maser observation results are tabulated.

3. Observation

The $J = 1{-}0$, $v = 1$ and 2 maser lines of SiO at the rest frequencies of 43.122 GHz and 42.821 GHz, respectively, were observed with the Nobeyama 45 m radio telescope during six sessions, 1998 May, June, 1999 June, and 2000 Apr., May, June. A cooled SIS receiver with a bandwidth of about 0.5 GHz was used. The aperture efficiency of the telescope was about 0.61 at 43 GHz. The half-power beam width (HPBW) was about $40''$ at 43 GHz.

An acousto-optical spectrometer array of a high resolution (AOS-H) was used. Each spectrometer has a 40 MHz bandwidth and 2048 frequency channels, giving the velocity coverage of about 280 km s^{-1} and the spectral resolution of 0.28 km s^{-1} (per two binned channels). For fear of missing high-velocity ($|V_{\rm LSR}| > 200$ km s^{-1}) components, a low resolution (AOS-W) array was also used. This has the velocity coverage of about 1700 km s^{-1} and the spectral resolution of 1.7 km s^{-1} (per two binned channels).

Observations were made in a position switching mode, where the off-position was chosen 5 arcmin away from the on-position in azimuth. The antenna temperature of the detection limit was 0.2 K at the 4 σ level. The system temperature (including atmospheric noise) was normally around 200 to 300 K, depending mainly on the weather condition and elevation angle of the antenna. The conversion factor from antenna temperature to flux density was 2.9 Jy K^{-1}.

The observations were made on the IRAS positions. Regular pointing checks and data calibration were made using the strong SiO maser sources, e.g., R LMi, U Her and W Hya etc. The pointing accuracy was usually found to be better than 10 arcsec.

We judged the detection of the SiO masers by the following criteria.

1. For a narrow spike-type emission, the peak antenna temperature must be greater than 10 σ and the line width greater than 6 channels (1.0 km s^{-1});
2. For broad emission, S/N must be larger than 10; the effective S/N is calculated from the half-power line width (the integrated intensity divided by half the peak intensity) and the average rms noise (corrected for the half-power line width).

4. Results and discussion

4.1. SiO maser detection rate

The SiO maser spectra of detected sources are displayed in Fig. 1. The observational results are summarized in Table 2 for detected sources and in Table 3 for non-detected sources. In Table 2, velocity in Local Standard of Rest frame (LSR), antenna temperature, the integrated flux, rms of the noise level and the date of observation in the format, YYMMDD.D are tabulated. In Table 3, rms of the noise level for each transition and observation date are tabulated. Stars marked "a" on the right shoulder of their IRAS name do not satisfy our selection criteria, but observed in the extra time, and are excluded from the later analysis.

Of the 97 sources in the North Galactic Cap, 16 had already been observed previously and had given 7 detections. Of the 83 sources observed in this survey, 17 detections are new. In total, SiO masers are detected in 24 out of the 97 sources, and the detection rate is about 25%. This value is much less than that of the previous surveys, 56% toward the near end of the Galactic bar (Izumiura et al. 1999), 62% toward the bulge (Jiang et al. 1995; Izumiura et al. 1994, 1995a, 1995b) and even less than 35% toward the outer disk (Jiang et al. 1996) even thouth the very similar color selection criteria and the same telescope was used.

This lower detection rate is partly attributed to the decrease of the number of oxygen-rich long-period Mira variables in the direction away from the Galactic plane. Distribution studies in the Galaxy suggest that the intermediate-period ($300^{\rm d} < P < 400^{\rm d}$) oxygen-rich Miras, that are most likely to emit SiO maser radiation, belong to the thin disk population (Jura & Kleinmann 1992a, 1992b; Kerschbaum & Hron 1992). On the other hand, short-period ($P < 300^{\rm d}$) oxygen-rich Miras or Semi-regular variables, that are on average farther from the Galactic plane and less likely to emit SiO masers, belong to the thick disk population (Jura 1994).

Table 1. Data of the sampled stars.

IRAS Name	l (deg)	b (deg)	C_{12}	C_{23}	LRS	SiO* (Y/N)	Period (days)	Distance (pc)	GCVS Name
08016+4107	179.4	30.7	−0.19	−0.74	29	Y		1678.1	
08020+6637	149.4	32.2	−0.25	−0.81		N		1818.5	
08134+4017	180.8	32.8	−0.18	−0.76		N	295.2	3862.5	W Lyn
08258+6237	153.9	35.2	−0.26	−0.84		N		2398.7	
08430+3705	185.8	38.0	−0.04	−1.05		N		4080.5	
09005+0824	221.0	33.0	−0.28	−0.67		N		1839.7	
09057+1325	216.2	36.3	−0.30	−0.75	15	N[a]		504.0	CW Cnc
09069+2527	201.9	40.7	−0.29	−0.76	23	Y[a]	393.2	721.4	W Cnc
09276+4454	175.5	46.6	0.18	−0.85		N[d]		3245.5	
09343−0536	240.5	32.6	−0.28	−0.67		N		2736.0	
09406+5359	161.9	46.7	−0.26	−1.02		N	326.0	1726.9	YY UMa
09439−0547	242.5	34.3	−0.29	−0.89		N		1681.9	TT Sex
10196+2545	207.1	56.7	−0.29	−0.90		N		957.3	
10353−1145	258.9	39.2	−0.24	−0.80		N	85.0	345.1	FF Hya
10411+6902	138.4	44.4	−0.23	−0.89	23	Y[a]	301.6	624.8	R UMa
10457+3633	185.8	62.4	−0.24	−0.82	15	N		1386.3	
10521+7208	134.7	42.5	−0.25	−0.68	26	Y	215.2	792.2	VX UMa
10594−0723	261.7	46.3	−0.20	−0.81		N	342.7	2758.0	RT Crt
11125+7524	130.8	40.5	−0.26	−0.85	23	Y		567.5	CS Dra
11193−2443	278.4	33.6	−0.24	−0.83		N		1158.0	
11252+1525	240.4	67.2	−0.19	−0.90		N	107.0	544.5	AF Leo
11269−1839	277.4	39.8	−0.30	−0.61		N		2621.5	
11443+5830	138.4	56.9	−0.24	−0.99		N		1813.5	WW UMa
11445+4344	157.2	69.1	−0.15	−0.90		N		917.8	AZ UMa
11472−0800	277.9	51.6	0.10	−0.90		N[d]		4239.8	
11567−2652	288.9	34.3	−0.20	−0.94	29	Y		1830.6	
12016+1903	248.0	76.3	−0.28	−0.68	24	Y[a]	362.8	1263.0	R Com
12020+0254	276.4	63.0	−0.22	−0.77	26	N	134.0	706.5	TZ Vir
12120−0545	286.5	55.7	−0.24	−0.73		Y[b]	339.5	1721.5	T Vir
12219−0445	290.5	57.2	−0.28	−0.68		N		1737.6	
12254+1904	268.7	80.1	−0.27	−0.95		N		1897.3	TV Com
12323−2033	297.7	41.9	−0.28	−0.76	14	N		1227.2	RU Crv
12326−2017	297.8	42.1	−0.29	−0.64		N		2220.0	
12344+2720	213.2	86.8	−0.30	−0.87		N[a]		553.5	
12449+3838	127.1	78.7	−0.18	−0.87	26	N[a]	345.6	1677.2	U CVn
12462+0738	301.0	70.2	−0.29	−0.63		N		2654.5	
12562+2324	325.6	85.7	−0.23	−0.73	28	N[a]	406.0	1253.6	T Com
12564−3125	304.8	31.1	−0.28	−0.66		N		2611.6	
13006−2850	306.1	33.7	−0.22	−0.77		N	218.8	2143.6	SW Hya
13053−3208	307.0	30.3	−0.27	−0.67		N		1953.0	
13245−2446	313.1	37.1	−0.26	−0.85	29	N		1657.8	
13252−0254	320.5	58.5	−0.27	−0.68		N	250.1	2489.7	V Vir
13326−2207	316.1	39.4	−0.28	−0.62		N		2852.7	
13367−3031	315.0	31.0	−0.24	−0.64		N	253.0	2954.1	V0603 Cen
13562−1342	326.8	45.8	−0.27	−0.62	14	N		1397.8	
13573+2801	39.4	74.9	−0.23	−0.78	22	N	120.0	765.0	WY Boo
13582+3806	73.8	72.0	−0.19	−0.77		N		1049.8	CY CVn
13594−0522	333.1	53.1	−0.29	−0.63		N	313.0	2851.6	AB Vir
14021−1909	325.8	40.2	−0.25	−0.72		N		2804.7	
14086−0730	334.8	50.1	−0.13	−0.78		Y[c]		707.0	IO Vir
14086−2839	323.4	30.8	−0.30	−0.74	26	N[a]	331.5	584.6	RU Hya
14142−1612	330.9	41.7	−0.27	−0.77	22	N		666.4	EW Vir
14247+0454	352.7	58.0	−0.22	−0.74	24	Y[a]	354.0	669.7	RS Vir
14257−0530	342.0	49.6	0.09	−0.76		N		7408.0	
14303−1042	339.2	44.7	−0.20	−0.82		Y		2350.2	
14371+3245	52.5	66.1	−0.25	−0.81	22	N[a]	137.0	319.1	RV Boo
14382−2504	332.1	31.3	−0.23	−0.81		N		2127.4	

Table 1. continued.

IRAS Name	l (deg)	b (deg)	C_{12}	C_{23}	LRS	SiO* (Y/N)	Period (days)	Distance (pc)	GCVS Name
14436−0703	346.0	45.8	−0.15	−0.77		N		4250.2	
14524−2148	337.4	32.5	−0.29	−0.73	24	Y	365.0	1280.8	EG Lib
14534−0359	351.6	46.6	−0.29	−0.71		N		2527.4	
14571−2135	338.6	32.0	−0.26	−0.76	29	Y		1821.5	
15060+0947	11.0	53.3	−0.12	−0.82	28	Y		1475.6	
15090−0549	353.8	42.6	−0.29	−0.81		Y	275.7	1389.5	Y Lib
15106−1532	346.0	35.0	0.16	−0.64		N		6178.7	
15114−0142	358.5	45.1	−0.26	−1.00	28	N	432.7	1497.6	Y Ser
15193+3132	49.5	57.2	−0.20	−0.81	24	Y[a]	360.3	528.1	S CrB
15194−1829	345.7	31.4	−0.28	−0.71	14	N		1356.6	
15223−0203	0.6	42.8	−0.18	−0.76	24	N		706.7	OV Ser
15250+2952	46.6	55.8	−0.27	−0.61		N		3020.3	
15255+1944	29.5	53.5	−0.19	−0.91	29	Y[a]	425.1	559.5	WX Ser
15262+0400	8.1	45.8	−0.17	−0.82	27	N[a]		1075.9	MW Ser
15334+2555	40.3	53.4	−0.25	−0.96	28	N	436.0	2176.6	RU CrB
15367+1044	18.4	47.3	−0.29	−0.81	29	N		1735.7	
15415+0232	9.6	41.9	−0.23	−0.73	14	N		1865.8	
15517−1043	358.6	31.6	−0.20	−0.65	14	N		1683.7	GP Lib
15522−0749	1.3	33.4	−0.26	−1.03		N		1816.9	
15540+0910	19.4	42.8	−0.11	−0.36		N	280.0	3282.0	RU Ser
15566+3609	57.6	49.6	−0.28	−0.92	26	Y	332.2	763.0	RS CrB
16030−0634	4.5	32.1	−0.26	−0.69		Y	340.4	2077.7	BD Oph
16037+4218	66.9	48.0	−0.22	−0.79	28	Y		1787.3	
16131−0216	10.4	32.6	−0.29	−0.76	24	Y		1213.8	
16211+3057	50.8	44.0	−0.24	−0.73	15	N	90.0	575.1	RY CrB
16241−0230	11.9	30.2	−0.22	−0.93	28	N		1739.3	V0707 Oph
16260+3454	56.4	43.5	−0.10	−0.68	28	N[a]		1176.7	V0697 Her
16293+4900	75.8	42.9	−0.21	−0.74		N		2534.9	
16330+0405	19.9	31.9	−0.24	−0.74		N		2754.0	
16400+3301	54.4	40.4	−0.29	−0.76	13	N		1417.3	
16418+5435	82.8	40.2	−0.28	−0.72		N		2024.3	
16418+5459	83.3	40.2	−0.25	−0.78	24	N	136.0	308.0	S Dra
16560+2252	43.1	34.5	−0.24	−0.72		Y	222.0	2174.3	MV Her
17050+1714	37.7	30.5	−0.22	−0.77	14	Y	300.4	2330.7	VY Her
17313+7033	101.2	32.2	−0.25	−0.72		N		2573.8	
17329+5359	81.6	32.8	−0.21	−0.72	25	Y	391.4	1297.8	SY Dra
17343+7601	107.5	31.0	−0.28	−0.90		N		2369.4	
17343+5026	77.4	32.4	−0.30	−0.67		N	370.0	2426.8	AO Her
17361+5746	86.1	32.5	−0.16	−0.78	28	N		940.6	TY Dra
17403+6234	91.8	32.0	−0.29	−0.74	15	N		1033.6	

Notes to Table 1:
l, b: Galactic longitude and latitude calculated from the IRAS position.
* SiO: SiO maser detection results. Y means "detection" and N means "non-detection" respectively.
[a] Benson et al. (1990).
[b] Jewell et al. (1991).
[c] Hall et al. (1990) did not detect SiO maser from this star, but in this work, we detect.
[d] Fujii et al. in prep. (private communication).

4.2. Detection vs. IRAS properties

From the 45 stars in our sample with LRS spectra, 11 belong to class 1n and 34 to class 2n. In those 45 stars, SiO emission was detected only from class 2n stars (17 out of 34), with one exception (IRAS 17050+1714). It follows that the presence of SiO masers is strongly correlated with the LRS class 2n, which indicates silicate emission at 10 μm.

In Fig. 2, we plotted both SiO maser detected and non-detected sources on the IRAS two-color diagram. The SiO maser detected stars are concentrated in a small area, the IIIa and VII regions as defined by Van der Veen & Habing (1988). These areas are characterized by variable stars with circumstellar shells.

In the sample of 97 stars, there are only four with C_{12} larger than 0.0 (4%). This fraction is quite low in

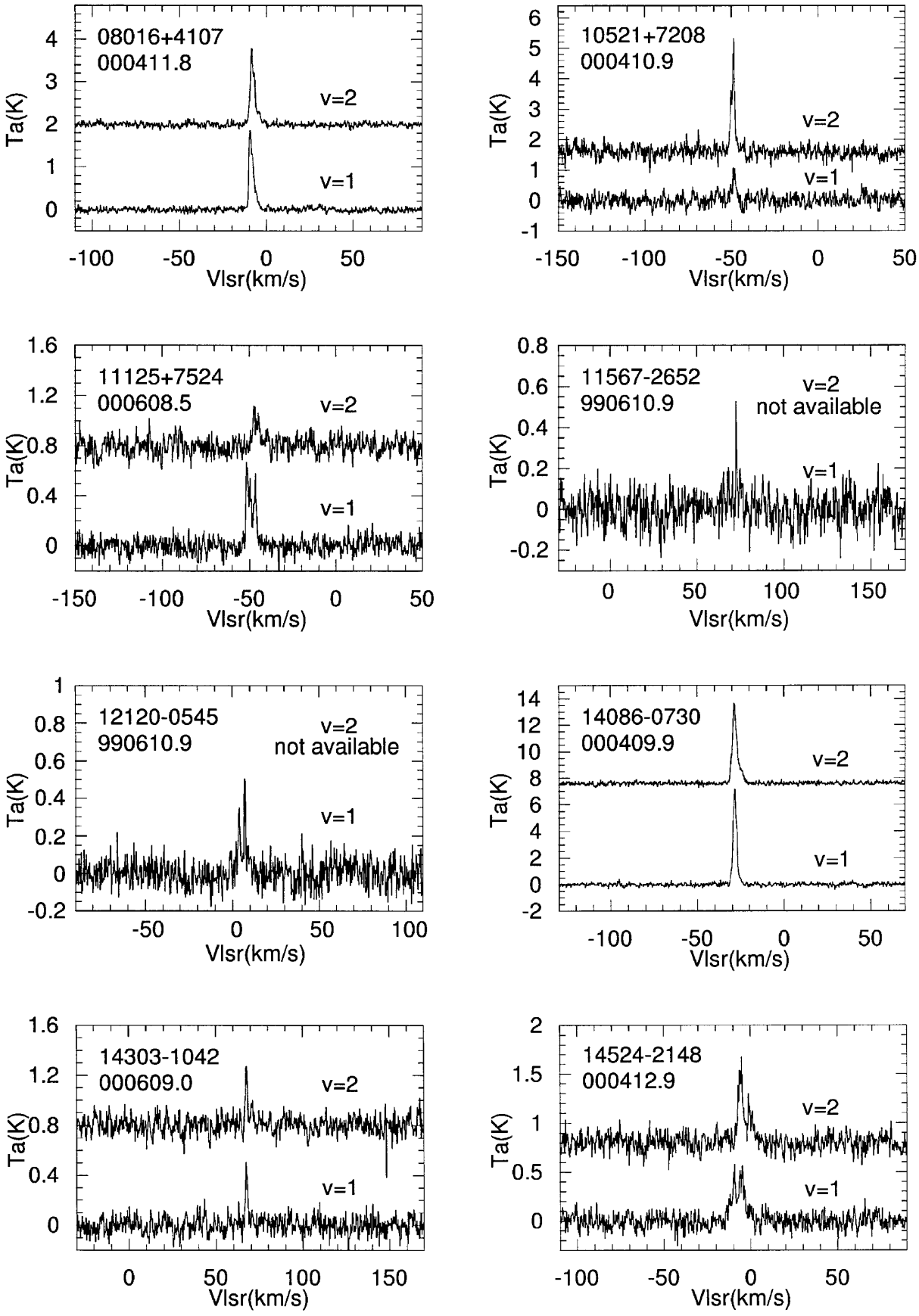

Fig. 1. Spectra of the SiO $J = 1{-}0$, $v = 1$ and 2 lines for detected sources.

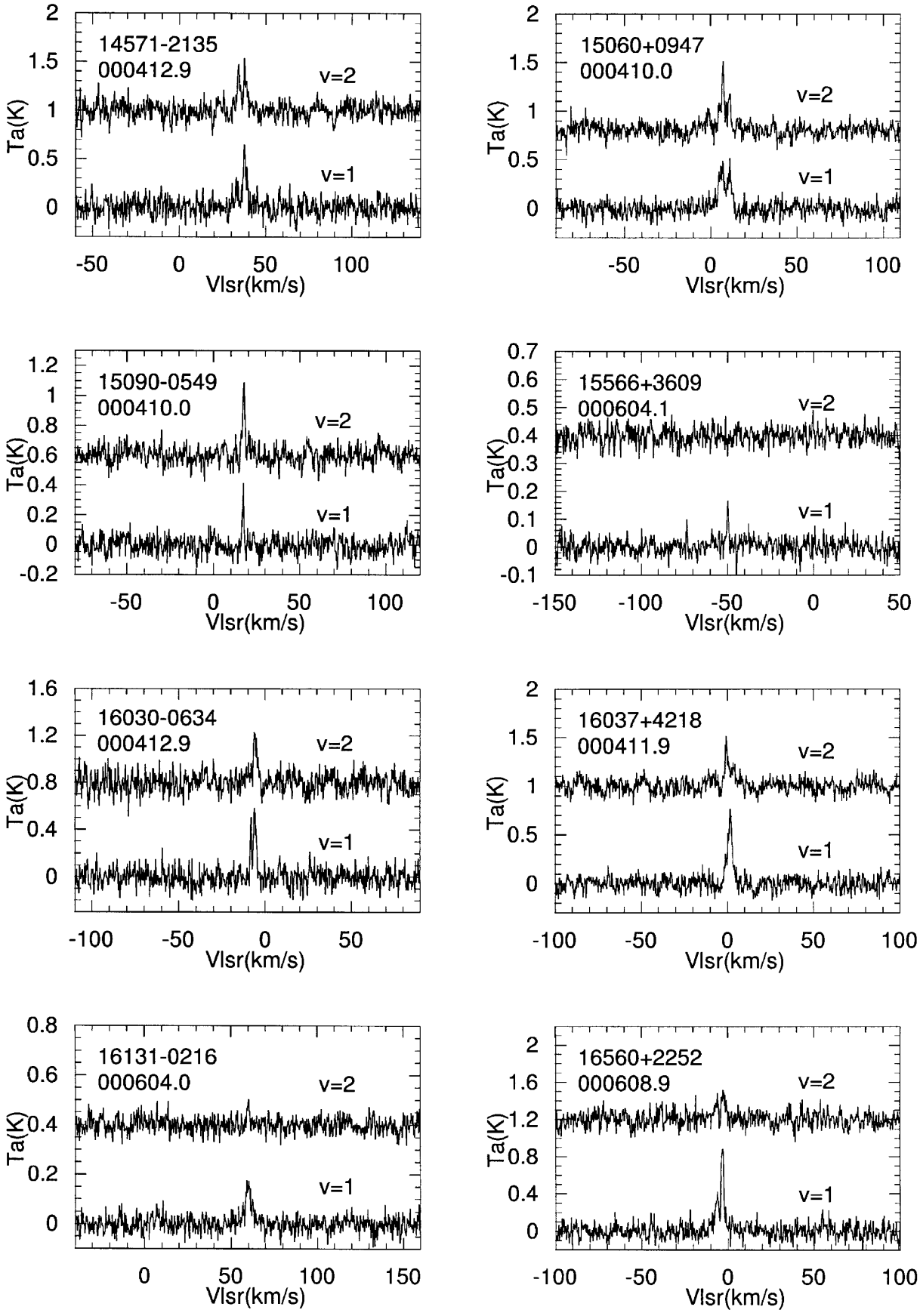

Fig. 1. continued.

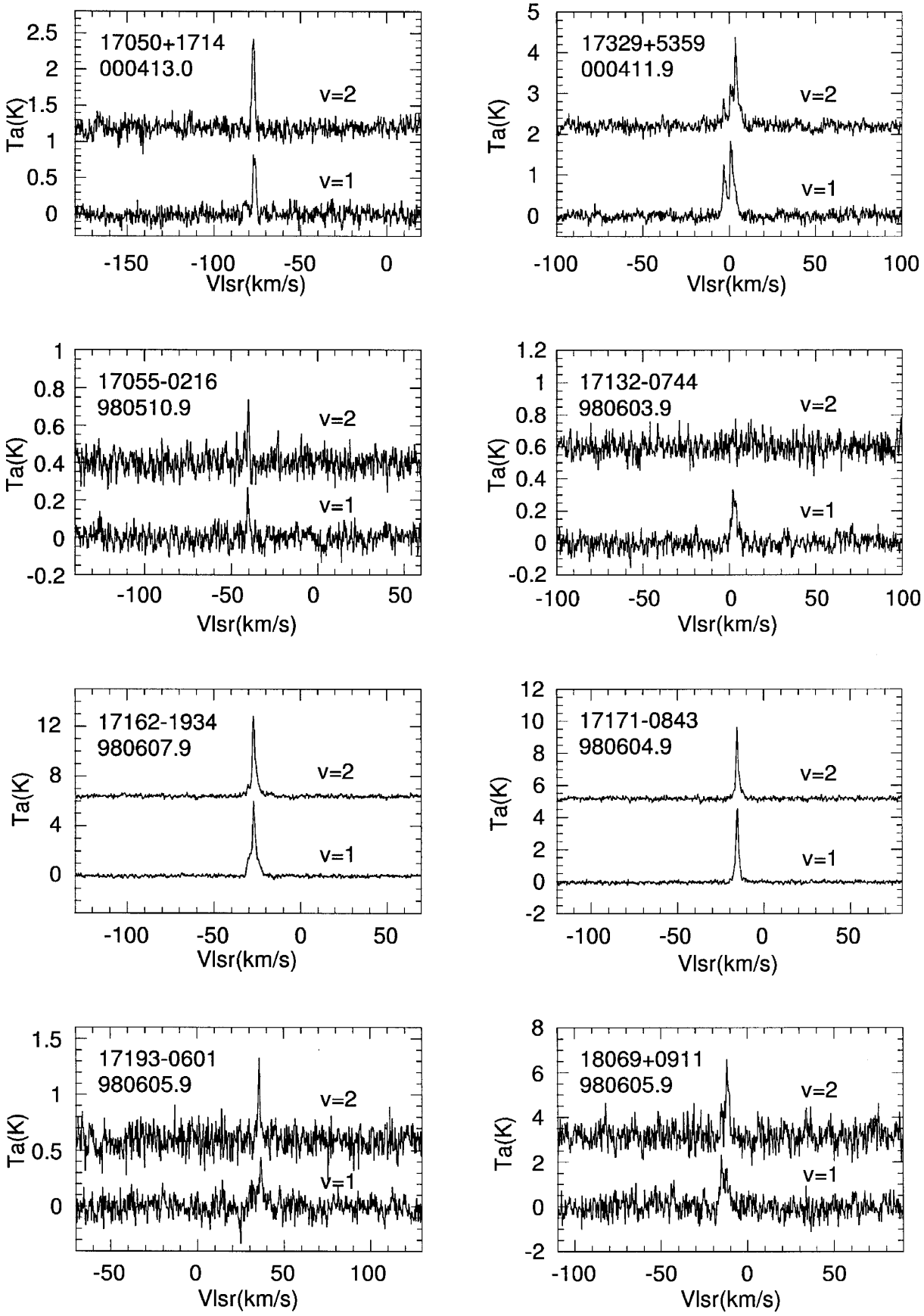

Fig. 1. continued.

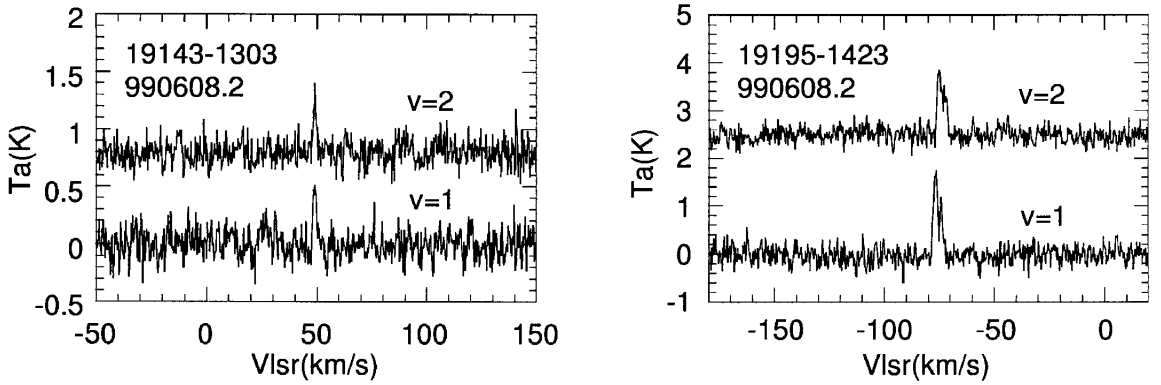

Fig. 1. continued.

Table 2. List of SiO maser detections.

	$J=1$–0, $v=1$				$J=1$–0, $v=2$				Observation
	$V_{\rm lsr}$	$T_{\rm a}$	S	rms	$V_{\rm lsr}$	$T_{\rm a}$	S	rms	date
IRAS Name	(km s^{-1})	(K)	(K km s^{-1})	(K)	(km s^{-1})	(K)	(K km s^{-1})	(K)	(yymmdd.d)
08016+4107	−9.3	1.875	5.899	0.047	−8.6	1.814	5.769	0.048	000411.8
10521+7208	−48.7	1.093	3.207	0.177	−48.6	4.005	8.198	0.171	000410.9
11125+7524	−51.7	0.668	2.640	0.058	−47.0	0.362	1.134	0.062	000608.5
11567−2652	72.5	0.529	1.133	0.075	—	—	—	—	990610.9
12120−0545	7.2	0.530	1.458	0.064	—	—	—	—	990610.9
14086−0730	−28.6	7.293	18.693	0.106	−28.8	6.073	21.210	0.103	000409.9
14303−1042	67.5	0.507	1.112	0.062	67.7	0.492	1.192	0.065	000609.0
14524−2148	−9.2	0.580	3.538	0.071	−5.0	0.876	3.689	0.078	000412.9
14571−2135	37.6	0.644	2.134	0.083	37.6	0.536	1.961	0.080	000412.9
15060+0947	11.0	0.560	3.028	0.065	7.2	0.713	3.042	0.065	000410.0
15090−0549	17.2	0.413	0.134	0.056	17.6	0.488	0.958	0.055	000410.0
15566+3609	−49.8	0.165	0.377	0.027	−51.1	0.069	−0.009	0.028	000604.1
16030−0634	−6.0	0.582	1.412	0.072	−6.4	0.443	1.164	0.082	000412.9
16037+4218	1.5	0.764	2.397	0.064	−0.8	0.516	2.011	0.064	000411.9
16131−0216	60.3	0.182	0.769	0.029	60.2	0.102	0.187	0.029	000604.0
16560+2252	−2.8	0.938	2.254	0.070	−2.8	0.316	0.870	0.075	000608.9
17050+1714	−76.6	0.839	2.228	0.081	−77.2	1.215	2.134	0.080	000413.0
17329+5359	1.0	1.825	8.121	0.090	3.6	2.177	8.460	0.097	000411.9
17055−0216[a]	−40.6	0.268	0.204	0.044	−40.1	0.379	0.310	0.052	980510.9
17132−0744[a]	2.1	0.332	1.007	0.048	3.7?	0.177	0.159	0.054	980603.9
17162−1934[a]	−27.2	6.140	19.528	0.086	−27.4	6.424	18.532	0.103	980607.9
17171−0843[a]	−15.5	4.542	9.914	0.239	−15.6	4.422	8.610	0.218	980604.9
17193−0601[a]	−36.5	0.437	1.415	0.081	−35.8	0.728	1.292	0.100	980605.9
18069+0911[a]	−15.1	2.309	7.119	0.396	−11.8	3.398	7.574	0.473	980605.9
19143−1303[a]	49.0	0.507	0.483	0.118	49.0	0.598	0.787	0.099	990608.2
19195−1423[a]	−75.0	1.857	4.784	0.197	−75.2	1.350	4.776	0.147	990608.2

Notes to Table 2:
[a]: These stars do not satisfy our selection criteria, and excluded from the following discussions.

comparison with the whole IRAS point sources. There are 6353 stars in the IRAS PSC which satisfy our color selection criteria and have $f_{12} > 3$ Jy. Among them, 1080 have C_{12} larger than 0.0 (17%). This may be interpreted as an indication that there are only a few massive AGB stars in the present high galactic latitude sample (Kwok 1990).

4.3. Spatial distribution

We used the following equation to calculate distances,

$$D_{\rm L} = \sqrt{L/(4\pi F_{\rm bol})} \quad (1)$$

where L is the luminosity of the star. The bolometric flux $F_{\rm bol}$ is calculated from the IRAS 12 μm flux f_{12} and bolometric correction factor BC,

$$F_{\rm bol}[{\rm W/m^2}] = 2.49 \times 10^{-13} \times BC \times f_{12}[{\rm Jy}]. \quad (2)$$

For O-rich stars, BC can be calculated by (van der Veen & Breukers 1989)

$$BC = 0.7 + 2.9{\rm e}^{-7.5\times C_{12}} + 0.9{\rm e}^{1.75\times C_{12}}. \quad (3)$$

In Eq. (3), C_{12} is the IRAS 12 and 25 μm flux density ratio, defined in Sect. 2.

Table 3. List of SiO maser non-detections.

	$J=1-0$, $v=1$	$J=1-0$, $v=2$	Observation		$J=1-0$, $v=1$	$J=1-0$, $v=2$	Observation
	rms	rms	date		rms	rms	date
IRAS Name	(K)	(K)	(yymmdd.d)	IRAS Name	(K)	(K)	(yymmdd.d)
08020+6637	0.054	0.045	000608.5	08134+4017	0.047	0.044	000411.8
08258+6237	0.051	0.045	000411.9	08430+3705	0.050	0.045	000608.5
09005+0824	0.056	0.050	000409.8	09276+4454[b]	0.050	0.048	000526.7
09343−0536	0.055	0.052	000409.8	09406+5359	0.043	0.045	000410.8
09439−0547	0.054	0.054	000526.6	10196+2545	0.066	0.064	000410.8
10353−1145	0.065	0.057	000608.6	10457+3633	0.045	0.044	000526.7
10594−0723	0.057	0.053	000409.9	11193−2443	0.085	0.083	000608.7
11252+1525	0.054	0.049	000409.9	11269−1839	0.060	0.057	000608.7
11443+5830	0.049	0.044	000411.9	11445+4344	0.072	0.072	000410.8
11472−0800[b]	0.051	0.050	000525.7	12020+0254	0.056	0.052	000409.9
12219−0445	0.066	0.061	000608.6	12254+1904	0.044	0.047	990607.8
12323−2033	0.065	0.055	000412.9	12326−2017	0.070	0.066	000608.7
12462+0738	0.043	0.045	990607.8	12564−3125	0.086	0.090	000609.9
13006−2850	0.065	0.071	990607.9	13053−3208	0.081	0.070	000412.9
13245−2446	0.078	0.070	000412.9	13252−0254	0.063	0.058	000409.9
13326−2207	0.057	0.068	000413.9	13367−3031	0.072	0.074	000518.9
13562−1342	0.074	0.071	000519.0	13573+2801	0.057	0.069	000413.9
13582+3806	0.192	0.187	000410.9	13594−0522	0.049	0.047	000410.0
14021−1909	0.041	0.040	990608.9	14142−1612	0.055	0.052	000609.9
14257−0530	0.048	—	990610.9	14382−2504	0.064	0.068	000609.9
14436−0703	0.079	0.078	000409.9	14534−0359	0.060	0.060	000609.0
15106−1532	0.037	0.034	990607.9	15114−0142	0.053	0.053	000410.0
15194−1829	0.057	0.058	000410.0	15223−0203	0.058	0.055	980513.9
15250+2952	0.067	0.062	000608.8	15334+2555	0.054	0.064	000413.9
15367+1044	0.051	0.046	000609.1	15415+0232	0.033	0.032	000604.0
15517−1043	0.090	0.106	000413.9	15522−0749	0.057	0.058	000603.9
15540+0910	0.057	0.042	980512.1	16211+3057	0.067	0.081	000413.9
16241−0230	0.061	0.062	000411.0	16293+4900	0.089	0.091	000608.8
16330+0405	0.081	0.070	000413.0	16400+3301	0.051	0.043	000608.8
16418+5435	0.066	0.061	000608.9	16418+5459	0.039	0.037	000604.1
17313+7033	0.054	0.050	000608.6	17343+5026	0.061	0.060	000411.9
17343+7601	0.076	0.066	000608.6	17361+5746	0.062	0.058	000608.9
17403+6234	0.064	0.053	000608.9	11331−1418[a]	0.126	—	990610.9
17038−2033[a]	0.112	0.092	980512.1	17093−1633[a]	0.135	0.118	980525.9
17221−1706[a]	0.084	0.071	980606.9	19083−0017[a]	0.053	0.059	990608.2
19094+0006[a]	0.077	0.087	990608.2	19386+0155[a]	0.040	0.036	990611.2
19438+0933[a]	0.037	0.031	990609.2	19457+0832[a]	0.037	0.034	990609.2
19583−0730[a]	0.039	0.032	990611.2				

Notes to Table 3:
[a] These stars do not satisfy our selection criteria, and excluded from the following discussions.
[b] T. Fujii et al. in prep. (private communication).

The luminosity of each star, L is calculated by using the period-bolometric magnitude relation for oxygen-rich Mira type variables (Van Leeuwen et al. 1997),

$$M_{\rm bol} = -3.00 \log P + 2.88 \quad (4)$$

and by adopting $M_{\odot{\rm bol}} = 4.72$ (Zombeck 1982), where $M_{\rm bol}$ and $M_{\odot{\rm bol}}$ are the absolute bolometric magnitude of each star and that of the Sun respectively. Pulsation periods have been found for 36 stars in the General Catalog of Variable Stars (GCVS) (Kholopov et al. 1992) and these are listed in Table 1. Their luminosities are calculated from the above equation. The median of the known periods is about 300 days. According to the above relation, a Mira type variable with the period of around 300 days would

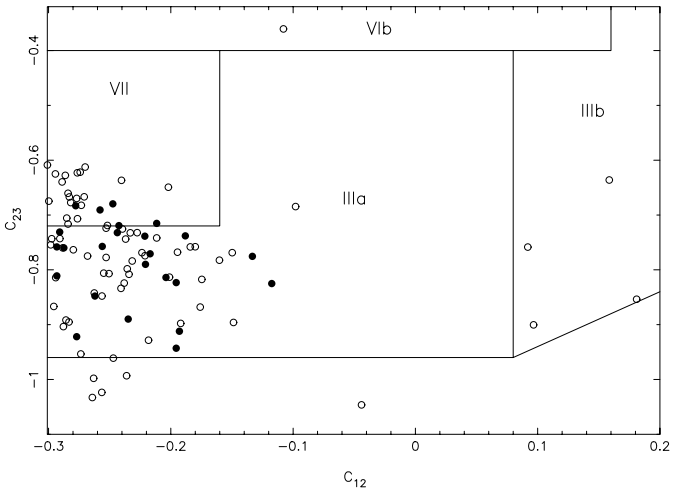

Fig. 2. IRAS two-color diagram of the present sample. The filled and open circles represent SiO detections and non-detections, respectively. Van der Veen & Habing (1988) studied IRAS sources based on a two-color diagram which they divided into 10 regions, and these are also included.

have a luminosity of about 5000 $L_{\odot}$. Thus, for the remaining 61 stars, we assumed that they all have the luminosity of 5000 $L_{\odot}$. Distances derived are tabulated in Table 1.

Having deduced the distance to the individual stars, we can then calculate the position of the stars in the heliocentric cartesian coordinates and look at their Galactic distribution, as shown in Fig. 3. There are more stars in the hemisphere towards the Galactic center (68 stars) than the anti-center (29 stars). To some extent, this trend comes from the effect that the number density of the star is falling with the Galactocentric radius. Among the SiO detected 24 stars, 18 are in the hemisphere towards the Galactic center and 6 are in the anti-center (see Fig. 3 middle and bottom). Thus the detection rate is 26% for the inner hemisphere and 20% for the outer one, respectively. However, there seems no such asymmetry in the yz plane (see Fig. 3 top). The difference in two proportions test showed that this asymmetry in detection rate is meaningful with the 72% confidence level, unfortunately within the statistical error.

The trend for the lower detection rate in the outer Galactic disk could be explained as the number ratio of carbon to oxygen-rich stars increases for larger Galactic radii (Jura 1993). Jura (1992c) found the remarkable increase of the fraction of carbon-rich red giants in the outer Milky Way. Jiang et al. (1999) concluded that the decreasing sequence of SiO maser population with the galactocentric distance is possibly as a consequence of a variation in the proportion of oxygen-rich variable stars and the galactic metallicity gradient. A decrease in metallicity as a function of Galactic radius has been suggested by Shaver et al. (1983) and the relationship between metallicity and the ratio of carbon to oxygen-rich stars has been reported for external galaxies (Iben & Renzini 1983; Richer 1989).

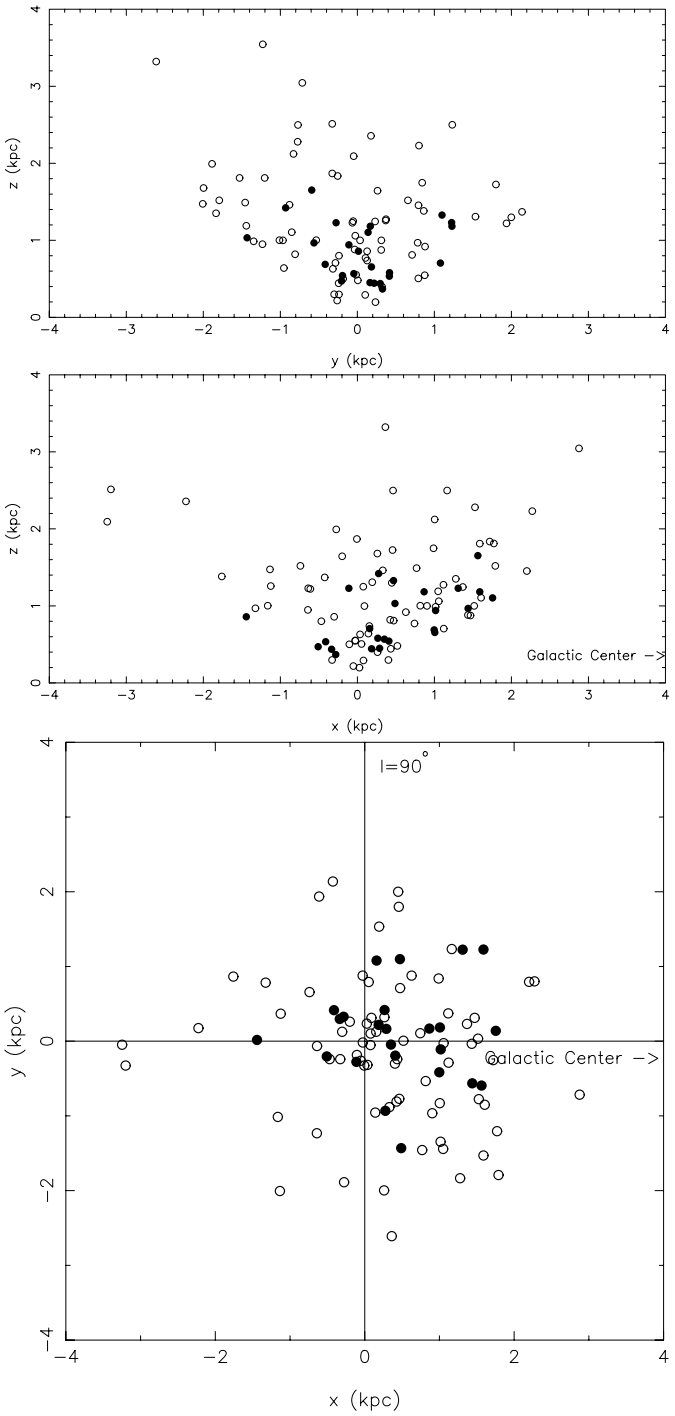

Fig. 3. The spatial distribution of stars in the heliocentric cartesian coordinates. The coordinates, x, y and z increase toward the Galactic center, anti Galactic rotation, and the North Galactic Pole, respectively. The filled circles represent SiO detections, and the open circles non-detections.

Figure 4 is a histogram of the distance from the Galactic plane (z) of the present sample. The hatched area shows the number of SiO maser detections in each bin. There are no SiO detections above 1.8 kpc from the Galactic plane. This may be an artifact of the distance estimation. If this is real however, it could be explained by

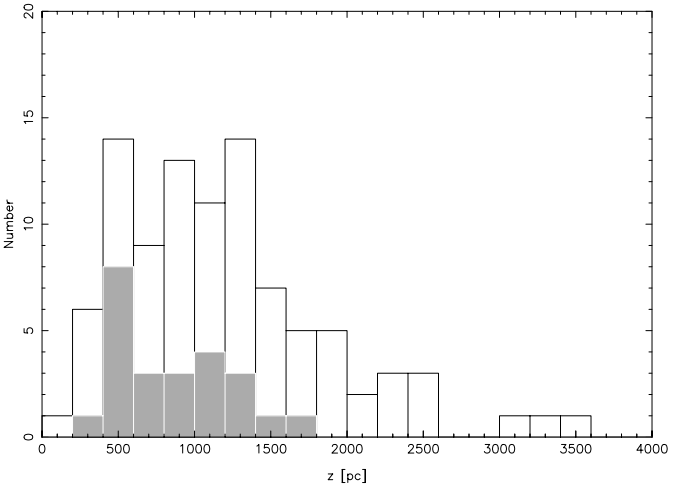

Fig. 4. Histogram of the Galactic height. The hatched area shows SiO maser detections, and the open area non-detections.

the metallicity gradient with the Galactic height. Norris & Green (1989) observed a well-defined vertical composition gradient, given formally by [Fe/H] $= -0.19\ z - 0.16$ (z in kpc). The lower metallicity away from the Galactic plane could lead to an increasing number of O-rich stars that turn into C-rich stars easily (Iben & Renzini 1983).

4.4. Galactic vertical kinematics

To investigate the Galactic vertical kinematics, the sample is limited to stars with distance, proper motions and l.o.s. velocities. Distances were derived from the method discussed in the Sect. 4.3. Proper motions were taken from the Tycho-2 catalog (Høg et al. 2000a, 2000b) and stellar identifications were made by matching IRAS positions and catalog positions when they differ less than 10 s of arc. High precision l.o.s velocities were derived for 24 stars from SiO maser observations and for the remaining 73 stars, literature was searched. These data are listed in Table 4.

The distances, proper motions, and l.o.s. velocities were converted into the space velocity components in the Galactocentric cylindrical coordinates. The azimuthal rotational component in the plane relative to a non-rotating point at the Solar position V_θ was calculated. The V_θ has been corrected for the peculiar motion of the Sun ($u_\odot = 8.1$, $v_\odot = 7.4$, $w_\odot = 6.4$) km s^{-1} (Ratnatunga & Arthur 1997) and 222 km s^{-1} (Kerr & Lynden-Bell 1986) as the azimuthal velocity of the LSR. A value of the distance to the Galactic center from the Sun of 8.5 kpc was adopted. Then we calculated the angular velocities (ω) around the Galactic center by dividing V_θ by Galactocentric distance of each star.

In Fig. 5, we plot angular velocity versus Galactic height. If the Milky Way has a discrete thick disk, there should be an extra branch of objects with a different $\omega - z$ relation. Because there are some uncertainties in the distance estimation and our subsample may not deep enough to contain much of thick disk population, the existence of some extra streams is not clear.

Table 4. Kinematical data.

IRAS name	Tycho-2 ID	$V_{\rm los}$ (km s^{-1})	$R_{\rm V}$	μ_α (mas/yr)	μ_δ
09069+2527	1954-01300-1	49.0	2	−15.70	−11.80
10353−1145	5495-00421-1	49.0	3	−52.70	−9.90
11125+7524	4549-01867-1	−50.0	1	−16.30	−13.80
11252+1525	1437-01509-1	6.0	3	−23.00	10.40
13252−0254	4962-00612-1	33.0	2	5.50	−4.20
14086−2839	6742-00806-1	2.0	2	−10.20	−32.30
14247+0454	0321-00490-1	−26.0	2	−6.70	1.90
14371+3245	2557-00818-1	−3.3	2	15.20	−5.70
15090−0549	5013-00562-1	17.4	1	−9.00	−18.60
15114−0142	5005-00784-1	−59.0	2	−31.60	−9.60
15193+3132	2563-01338-1	−1.0	2	−9.70	−15.90
15334+2555	2029-01030-1	−27.0	2	−7.40	−10.80
15566+3609	2578-00824-1	−50.2	1	−51.60	0.30
16211+3057	2580-00057-1	28.0	3	−17.30	6.10
16418+5459	3879-01661-1	6.0	2	3.30	−32.30
16560+2252	2059-00770-1	−2.8	1	3.60	−5.20

Notes to Table 4:
ID: Tycho-2 ID number.
$V_{\rm los}$: Line of sight velocity.
$R_{\rm V}$: Reference of the l.o.s. velocity.
1: This study.
2: General Catalogue of Stellar Radial Velocities (Wilson 1953).
3: The kinematics of semiregular red variables in the solar neighborhood (Feast et al. 1972).
μ_α, μ_δ: Proper motion in RA and DEC.

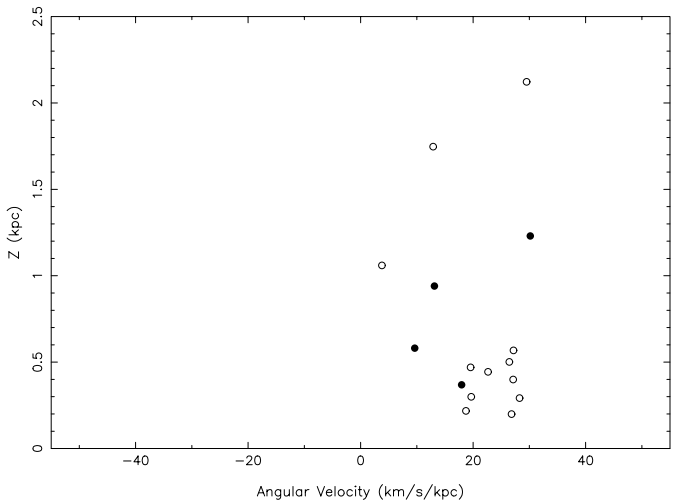

Fig. 5. The variation of angular velocity with the Galactic height. The filled circles indicate the stars of their l.o.s. velocities were determined by this study, and the open circles, data taken from the literature.

5. Conclusions

We have observed color-selected IRAS sources in the North Galactic Cap, in the SiO $J = 1{-}0$ $v = 1$ and 2 transitions, leading to 24 detections, of which 17 were new detections. The detection rate (about 25%) was quite low. This is possibly a consequence of a variation in the Galactic metallicity and hence the decreasing proportion of oxygen-rich long period variables that are most likely to emit SiO masers. No SiO masers were found from the stars with the Galactic height larger than 1.8 kpc in the present survey. We do not find any clear evidence for the existence of the extra branch in the $\omega{-}z$ plane.

Acknowledgements. It is a pleasure to thank Dr. H. Mito for useful and helpful discussions. This research has made use of the SIMBAD database operated at CDS, Strasbourg, France and partially based on data from the ESA Hipparcos astrometry satellite.

References

Benson, P. J., Little-Marenin, I. R., Woods, T. C., et al. 1990, ApJS, 74, 911
Cohen, R. J. 1989, Rep. Prog. Phys., 52, 881
Deguchi, S., & Iguchi, T. 1976, PASJ, 28, 307
ESA 1997, The Hipparcos and Tycho Catalogs, ESA, SP 1200
Feast, M. W., Woolley, R., & Yilmaz, N. 1972, MNRAS, 158, 23
Kholopov, P. N., Samus, N. N., Durlevich, O. V., et al. 1992, General catalogue of variable stars, fourth edition (Bull. Inf. Centre Données Stellaires)
Hall, P. J., Allen, D. A., Troup, E. R., et al. 1990, MNRAS, 243, 480
Høg, E., Fabricius, C., Makarov, V. V., et al. 2000a, A&A, 357, 367
Høg, E., Fabricius, C., Makarov, V. V., et al. 2000b, A&A, 355, L27
Iben, I., & Renzini, A. 1983, ARA&A, 21, 271
IRAS Science Team 1988, IRAS Point Source Catalog, Version 2
Izumiura, H., Deguchi, S., Hashimoto, O., et al. 1994, ApJ, 437, 419
Izumiura, H., Catchpole, R., Deguchi, S., et al. 1995a, ApJS, 98, 271
Izumiura, H., Deguchi, S., Hashimoto, O., et al. 1995b, ApJ, 453, 837
Izumiura, H., Deguchi, S., Fujii, T., et al. 1999, ApJS, 125, 257
Jewell, P. R., Snyder, L. E., Walmsley, C. M., et al. 1991, A&A, 242, 211
Jiang, B. W., Deguchi, S., Izumiura, H., et al. 1995, PASJ, 47, 815
Jiang, B. W., Deguchi, S., Yamamura, I., et al. 1996, ApJS, 106, 463
Jiang, B. W., Deguchi, S., & Ramesh, B. 1999, PASJ, 51, 95
Jura, M., & Kleinmann, S. G. 1992a, ApJS, 83, 329
Jura, M., & Kleinmann, S. G. 1992b, ApJS, 79, 105
Jura, M. 1992c, A&AR, 2, 227
Jura, M., & Yamamoto, A. 1993, ApJ, 413, 298
Jura, M. 1994, Ap&SS, 217, 101
Kerr, F. J., & Lynden-Bell, D. 1986, MNRAS, 221, 1023
Kerschbaum, F., & Hron, J. 1992, A&A, 263, 97
Kwok, S. 1990, MNRAS, 244, 179
Lane, A. P., Johnston, K. J., Spencer, J. H., et al. 1987, ApJ, 323, 756
Miyoshi, M., Matsumoto, K., Kameno, S., et al. 1994, Nature, 371, 395
Nakada, Y., Onaka, T., Yamamura, I., et al. 1993, PASJ, 45, 179
Norris, J. E., & Green, E. M. 1989, ApJ, 337, 272
Ratnatunga, K. U., & Upgren, A. R. 1997, AJ, 476, 811
Richer, H. B. 1989, IAU Coll. 106 (Cambridge University Press), 35
Shaver, P. A., McGee, R. X., Newton, L. M., et al. 1983, MNRAS, 204, 53
van der Veen, W. E. C. J., & Habing, H. J. 1988, A&A, 194, 125
van der Veen, W. E. C. J., & Breukers, R. J. L. H. 1989, A&A, 213, 133
van Leeuwen F., Feast, M. W., Whitelock, P. A., & Yudin, B. 1997, MNRAS, 287, 955
Whitelock, P., Menzies, J., Feast, M., et al. 1994, MNRAS, 267, 711
Wilson, R. E. 1953, Carnegie Inst. Washington DC, Publ. 601
Zombeck, Martin, V. 1982 (Cambridge University Press), 102